A rate threshold mechanism regulates MAPK stress signaling and survival

Amanda N. Johnson[a], Guoliang Li[a], Hossein Jashnsaz[a], Alexander Thiemicke[a], Benjamin K. Kesler[a], Dustin C. Rogers[a], and Gregor Neuert[a,b,c,1]

[a]Department of Molecular Physiology and Biophysics, School of Medicine, Vanderbilt University, Nashville, TN 37232; [b]Department of Pharmacology, School of Medicine, Vanderbilt University, Nashville, TN 37232; and [c]Department of Biomedical Engineering, School of Engineering, Vanderbilt University, Nashville, TN 37232

Edited by Natalie G. Ahn, University of Colorado, Boulder, CO, and approved November 24, 2020 (received for review March 19, 2020)

Cells are exposed to changes in extracellular stimulus concentration that vary as a function of rate. However, how cells integrate information conveyed from stimulation rate along with concentration remains poorly understood. Here, we examined how varying the rate of stress application alters budding yeast mitogen-activated protein kinase (MAPK) signaling and cell behavior at the single-cell level. We show that signaling depends on a rate threshold that operates in conjunction with stimulus concentration to determine the timing of MAPK signaling during rate-varying stimulus treatments. We also discovered that the stimulation rate threshold and stimulation rate-dependent cell survival are sensitive to changes in the expression levels of the Ptp2 phosphatase, but not of another phosphatase that similarly regulates osmostress signaling during switch-like treatments. Our results demonstrate that stimulation rate is a regulated determinant of cell behavior and provide a paradigm to guide the dissection of major stimulation rate dependent mechanisms in other systems.

signal transduction | rate threshold | single cell | systems biology

All cells employ signal transduction pathways to respond to physiologically relevant changes in extracellular stressors, nutrient levels, hormones, morphogens, and other stimuli that vary as functions of both concentration and rate in healthy and diseased states (1–7). Switch-like "instantaneous" changes in the concentrations of stimuli in the extracellular environment have been widely used to show that the strength of signaling and overall cellular response are dependent on the stimulus concentration, which in many cases needs to exceed a certain threshold (8, 9). Previous studies have shown that the rate of stimulation can also influence signaling output in a variety of pathways (10–17) and that stimulation profiles of varying rates can be used to probe underlying signaling pathway circuitry (4, 18, 19). However, it is still not clear how cells integrate information conveyed by changes in both the stimulation rate and concentration in determining signaling output. It is also not clear if cells require stimulation gradients to exceed a certain rate in order to commence signaling.

Recent investigations have demonstrated that stimulation rate can be a determining factor in signal transduction. In contrast to switch-like perturbations, which trigger a broad set of stress-response pathways, slow stimulation rates activate a specific response to the stress applied in *Bacillus subtilis* cells (10). Meanwhile, shallow morphogen gradient stimulation fails to activate developmental pathways in mouse myoblast cells in culture, even when concentrations sufficient for activation during pulsed treatment are delivered (12). These observations raise the possibility that stimulation profiles must exceed a set minimum rate or rate threshold to achieve signaling activation. Although such rate thresholds would help cells decide if and how to respond to dynamic changes in stimulus concentration, the possibility of signaling regulation by a rate threshold has never been directly investigated in any system. Further, no study has experimentally examined how stimulation rate requirements impact cell phenotype or how cells molecularly regulate the stimulation rate required for signaling activation. As such, the biological significance of any existing rate threshold regulation of signaling remains unknown.

The budding yeast *Saccharomyces cerevisiae* high osmolarity glycerol (HOG) pathway provides an ideal model system for addressing these issues (Fig. 1*A*). The evolutionarily conserved mitogen-activated protein kinase (MAPK) Hog1 serves as the central signaling mediator of this pathway (20–22). It is well established that instantaneous increases in osmotic stress concentration induce Hog1 phosphorylation, activation, and translocation to the nucleus (18, 21, 23–30). Activated Hog1 governs the majority of the cellular osmoadaptation response that enables cells to survive (23, 31, 32). Multiple apparently redundant MAPK phosphatases dephosphorylate and inactivate Hog1, which, along with the termination of upstream signaling after adaptation, results in its return to the cytosol (Fig. 1*A*) (23, 25, 26, 33–39). Because of this behavior, time-lapse analysis of Hog1 nuclear enrichment in single cells has proven an excellent and sensitive way to monitor signaling responses to dynamic stimulation patterns in real time (18, 27–30, 40, 41). Further, such assays have been readily combined with traditional growth and molecular genetic approaches to link observed signaling responses with cell behavior and signaling pathway architecture (27–29).

Here, we use systematically designed osmotic stress treatments imposed at varying rates of increase to show that a rate threshold

Significance

Signaling pathways must decide how to respond to extracellular stimulation patterns that vary widely in vivo. However, most experiments only explore how cells respond to one stimulation variable: concentration. By probing the model yeast osmostress mitogen-activated protein kinase pathway with diverse stimulation gradients we explore cellular sensitivity to multiple stimulation variables. We identify a rate threshold required for signaling and show that the timing of signaling initiation depends on both stimulation rate and concentration in finite-rate treatments. We connect our discovered limit on cell sensitivity to stimulation rate with a phenotype and molecular mechanism, demonstrating its biological relevance. Our results provide motivation and a blueprint for the dissection of other major stimulation-rate-dependent mechanisms in a variety of systems.

Author contributions: A.N.J. and G.N. designed research; A.N.J., G.L., H.J., and G.N. performed research; A.N.J., A.T., B.K.K., D.C.R., and G.N. contributed new reagents/analytic tools; A.N.J., H.J., and G.N. analyzed data; and A.N.J. and G.N. wrote the paper.

The authors declare no competing interest.

This article is a PNAS Direct Submission.

[1]To whom correspondence may be addressed. Email: gregor.neuert@vanderbilt.edu.

This article contains supporting information online at https://www.pnas.org/lookup/suppl/doi:10.1073/pnas.2004998118/-/DCSupplemental.

Published December 21, 2020.

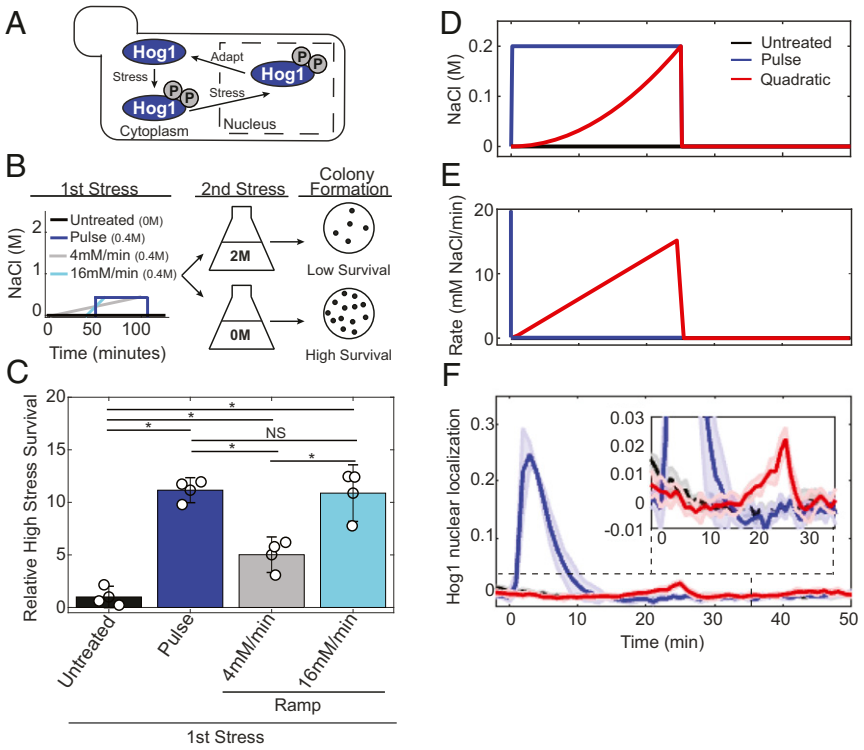

Fig. 1. Hog1 signaling and cell survival are sensitive to the rate of preconditioning osmotic stress application. (*A*) Schematic of the budding yeast HOG response. (*B*) Preconditioning protection assay workflow indicating the first stress treatments to a final concentration of 0.4 M NaCl (*Left*), high-stress exposure (*Middle*), and colony formation readout (*Right*). (*C*) High-stress survival as a function of each first treatment relative to the untreated first stress condition. Bars and errors are means and SD from three biological replicates. *Statistically significant by Kolmogorov–Smirnov test ($P < 0.05$). NS = not significant. (*D*) Treatment concentration over time. (*E*) Treatment rate over time for quadratic and pulse treatment. The rate for the pulse is briefly infinite (blue vertical line) before it drops to 0. (*F*) Hog1 nuclear localization during the treatments depicted in *D* and *E*. (*Inset*) Localization pattern in the quadratic-treated sample. Lines represent means and shaded error represents the SD from three to four biological replicates.

condition regulates yeast high-stress survival and Hog1 MAPK signaling. We demonstrate that only stimulus profiles that satisfy both this rate threshold condition and a concentration threshold condition result in robust signaling. We go on to show that the protein tyrosine phosphatase Ptp2, but not the related Ptp3 phosphatase, serves as a major rate threshold regulator. By expressing *PTP2* under the control of a series of different enhancer–promoter DNA constructs, we demonstrate that changes in the level of Ptp2 expression can alter the stimulation rate required for signaling induction and survival. These findings establish rate thresholds as a critical and regulated component of signaling biology akin to concentration thresholds.

Results

Stimulus Treatment Rate Affects Yeast High Osmotic Stress Survival and Hog1 Nuclear Translocation Pattern. We hypothesized that a rate threshold governs the budding yeast HOG pathway. The existence of such a threshold would place a minimum stimulation rate on osmoadaptation. Shallow rates of stimulation that fall below this minimum would not result in a robust osmoadaptive response, even if the same stimulus concentration triggered a response when applied at a faster rate.

To test this hypothesis, we first took advantage of the fact that preexposure to a mild pulsed stress treatment increases the stress tolerance of yeast through induction of the osmoadaptive response (42–44). This increased tolerance enables cells to survive a second, otherwise lethal, high-stress pulse treatment (42, 43). This preconditioning protection paradigm enables us to examine the rate dependence of mild stress responses independent of whether the stresses themselves differentially impact cell fitness.

Cells were initially exposed to preconditioning osmostresses (400 mM NaCl final concentration, equivalent integrated osmolarity) delivered at different rates. The impact of these preconditioning treatments on high-stress susceptibility was determined by comparing the viability of cells after a second transient high-stress treatment and no stress treatment (2 M and 0 M NaCl) (Fig. 1*B*). No substantial difference in growth was observed among the preconditioned cultures immediately following the initial treatments (*SI Appendix*, Fig. S1). However, the rate of preconditioning stress delivery profoundly influenced cell survival after the second high stress; cells exposed to a slow-rate treatment (4 mM NaCl/min [gray]) were significantly more sensitive to a high second stress than cells exposed to faster-rate treatments (16 mM NaCl/min [cyan] or pulse [blue], Fig. 1*C*). Further, extending the time cells were exposed to the final concentration of 0.4 M by an additional 60 min did not improve the high second-stress survival of cells preconditioned with the slow-rate treatment (*SI Appendix*, Fig. S2).

To investigate the mechanism(s) underlying the priming of high second-stress survival in response to variations in preconditioning stimulation rate, we tracked the nuclear enrichment of Hog1-yellow fluorescent protein (YFP), a proxy for canonical salt-stress signaling activation, during rate-varying stress treatments via single-cell time-lapse microscopy. Because previously published studies show that Hog1 nuclear translocation follows changing external stress patterns in real time (29, 30, 40), we began probing the relationship between stimulation rate and translocation using a stress treatment applied as a quadratic function (linearly increasing rate over time) (Fig. 1 *D* and *E*). Compared to pulse treatment, quadratic treatment resulted in an unprecedented delayed and diminished Hog1 nuclear accumulation response (Fig. 1*F*). Stimulation rate thus strongly influences signaling as well as high-stress

survival phenotype, consistent with expectations based on rate threshold regulation of the HOG pathway.

A Rate Threshold Regulates Hog1 Nuclear Enrichment. The Hog1 quadratic stimulation response pattern could be related to either a proposed stimulus concentration threshold requirement (25) or stimulation rate, since both are changing over time (Fig. 2 *A* and *B*). To investigate these relationships, Hog1 nuclear localization during the quadratic stress gradient was reanalyzed separately as a function of either the treatment concentration or rate. The concentration and rate corresponding with nuclear enrichment were extrapolated using two intersecting lines fitting Hog1 nuclear localization baseline and accumulation increase for each independent experiment. The thresholds for Hog1 translocation were 117.5 ± 34.5 mM NaCl and 12.1 ± 1.6 mM NaCl/min, respectively (Fig. 2 *A* and *B*). Surprisingly, the concentration associated with nuclear accumulation was much higher than the 50 to 70 mM salt expected based on published switch-like treatment responses measured via well-established immunoblotting assays (25, 27). This result raises the possibility that the rate of stress change drives Hog1 nuclear enrichment pattern during quadratic stimulation.

To systematically test if ∼12 mM NaCl/min represents an unreported rate threshold requirement for signaling we exposed cells to linear ramp treatments delivered at rates above, at, and below 12 mM NaCl/min (Fig. 2 *C* and *D*). Only ramps with rates greater than 12 mM NaCl/min resulted in detectable, albeit slightly delayed, Hog1 translocation (Fig. 2*E*). This result directly demonstrates that stimulus profiles must exceed a rate threshold to induce Hog1 nuclear enrichment.

Hog1 Translocation Requires Both the Rate and Concentration Thresholds. If stimulation rate solely determines signaling response, all ramps with gradients steeper than the rate threshold should bring about Hog1 translocation at the onset of treatment. Instead, we observed a delay in translocation in the 16 mM NaCl/min and 20 mM NaCl/min ramp treatments (Fig. 2*E*). Previously published data also show a lag in nuclear translocation during ramp treatment (28), although the corresponding report does not discuss this observation. Reanalyzing translocation during our ramp treatments that resulted in Hog1 nuclear localization as a function of concentration revealed that the timing of translocation in both activating ramps was associated with 57 ± 14.5 mM NaCl (*SI Appendix*, Fig. S3). This value agrees with the anticipated concentration threshold of 50 to 70 mM salt.

To directly test if 57 ± 14.5 mM NaCl serves as a concentration threshold condition in our system, we exposed cells to a switch-like change to a final concentration well below this threshold (30 mM NaCl). We observed a low level of Hog1 nuclear translocation during this treatment (*SI Appendix*, Fig. S4 *A–C*), consistent with another study that measured Hog1 activity via time-lapse microscopy instead of immunoblot (45). Thus, the 57 ± 14.5 mM NaCl is the concentration that is simply associated with translocation in finite rate treatments that exceed the rate threshold rather than an absolute concentration required for activation. We will henceforth refer to this value as the concentration term.

These results suggest that during finite rate treatments Hog1 nuclear accumulation pattern is set by the rate threshold and the concentration term (Fig. 2*F*). Yeast cell stress signaling responses to such treatments thus appear to follow AND logic where the output (signaling) occurs only once both input conditions (the rate threshold and concentration term) are met. In this model, slow increases in NaCl fail to trigger signaling. Meanwhile, both the rate threshold and concentration term determine the timing of Hog1 translocation in stimulus treatments that exceed the rate threshold, and Hog1 translocation corresponds with whichever condition was met last. The activating ramps exceed the rate threshold before the concentration term such that the timing of Hog1 translocation corresponds with the concentration term (Fig. 2 *C–F* and *SI Appendix*, Fig. S3). Meanwhile in our quadratic stimulation, the order in which these conditions are met is flipped and nuclear accumulation corresponds with the rate threshold instead (Fig. 2 *G–J*).

To further probe our AND logic model, we examined Hog1 nuclear translocation using additional and specifically designed quadratic stimulation patterns. These quadratic stimulation patterns enable the dissection of the concentration term, the rate threshold, and their AND logic relationship. As in the original quadratic perturbation, two of these stimulus profiles satisfy the concentration term before the rate threshold (*SI Appendix*, Fig. S5 *A* and *B*). The other two satisfy the rate threshold before the concentration term (*SI Appendix*, Fig. S6). As in the original quadratic stimulation, there is a noticeable time lag between the onset of stimulation and Hog1 nuclear accumulation in all treatments (*SI Appendix*, Figs. S5 *A–C* and S6). Hog1 translocation corresponds with very different NaCl concentrations in the first two quadratic gradients (*SI Appendix*, Fig. S5*D*). However, it corresponds with very similar rates (*SI Appendix*, Fig. S5*E*), which are of comparable value to the rate threshold identified in our original quadratic gradient (Fig. 2*B* and *SI Appendix*, Figs. S5*E* and S7*A*), consistent with expectations based on our AND logic model (Fig. 2*J*). Also, in agreement with this model, Hog1 translocation in the other two quadratic treatments corresponds with the concentration term and very different rates (*SI Appendix*, Figs. S4, S6, and S7).

As final tests of our model, we probed cells with four more stimulation profiles. The first three treatments (two ramps and one quadratic stimulation profile from 0.2 M to 0.4 M NaCl) were designed to explore how the absolute salt concentration affects the rate threshold and concentration term (*SI Appendix*, Fig. S4). The fourth was a very fast ramp (80 mM/min) that promptly satisfies both conditions (*SI Appendix*, Fig. S8). Hog1 translocation during all three 0.2 M to 0.4 M NaCl stimulation profiles exhibited a pattern consistent with the concentration term and rate threshold regulation (*SI Appendix*, Fig. S7 *A* and *B*). Meanwhile, the 80 mM/min ramp induced Hog1 nuclear localization at its onset (*SI Appendix*, Fig. S8). As with our previous results, this outcome is consistent with our model. We would expect rapid translocation when both conditions are satisfied at essentially the same time. However, it also underscores the fact that without a significant difference in the time each condition is met a single stimulation is insufficient to detect and/or measure either of them.

Identification of a Rate Threshold Regulator. The existence of a rate threshold raises the possibility of a rate threshold regulator. The ideal regulator would prevent Hog1 from responding when stimulation patterns fail to reach the rate threshold without impinging on the concentration term. To identify such a regulator, we first considered key modulators of Hog1 function (Fig. 3*A*). We specifically focused on the protein tyrosine phosphatases Ptp2 and Ptp3, which act as partially redundant Hog1 off switches during instantaneous changes in stress concentration (23, 33, 35), because these factors counteract phosphorylation of the Hog1 tyrosine residue (Tyr-176) required for salt-induced Hog1 activity (46).

We hypothesized that the deletion of Ptp2 and/or Ptp3 would remove a barrier to stimulus-induced Hog1 activation in stress treatments that exceed the concentration term but fall below the rate threshold. To test this hypothesis, we examined Hog1 nuclear accumulation patterns in wild-type (*WT*), *ptp2Δ*, and *ptp3Δ* yeast strains during our original quadratic stimulation, in which reduction or removal of the rate threshold would enable translocation earlier in the treatment time course according to the AND logic model (Fig. 3 *B–D*). While the pattern of Hog1 nuclear accumulation in *ptp3Δ* cells appeared similar to *WT* during

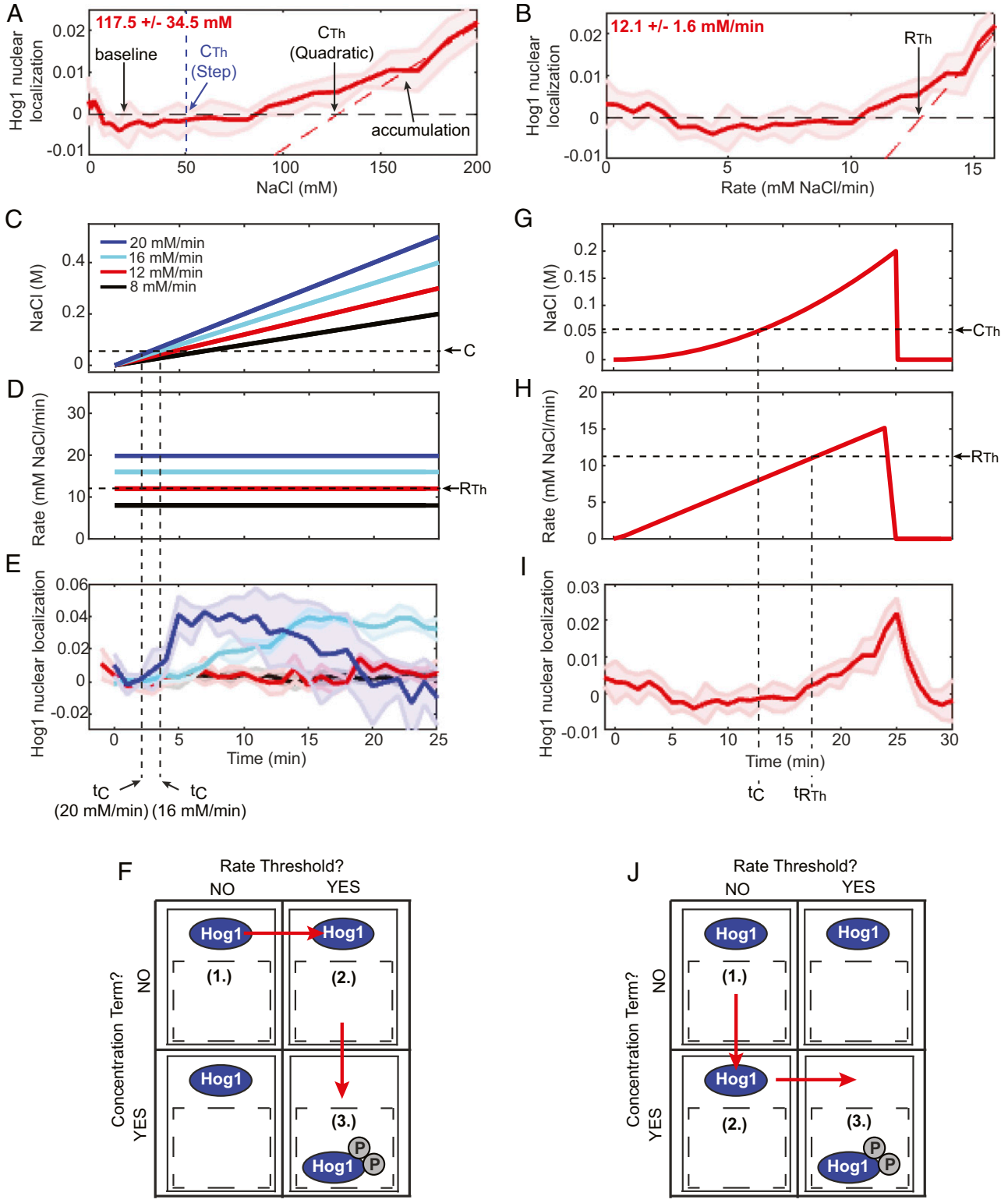

Fig. 2. A rate threshold condition regulates signaling nuclear localization. (*A*) Quadratic signaling response from Fig. 1*F* plotted as a function of treatment concentration. The intersection points between the dashed lines representing Hog1 nuclear localization baseline (black) and accumulation pattern either expected based on previously published immunoblot results (blue) or measured in quadratic treatment (red) indicate concentration thresholds (C_{Th}). The apparent quadratic C_{Th} is listed in bold red font. (*B*) Quadratic treatment response from Fig. 1*F* plotted as a function of treatment rate. A rate threshold (R_{Th}) (bold red font) was identified via the approach used for C_{Th} determination. (*C*) NaCl concentration change during ramp treatments. The concentration term "C" is marked. (*D*) NaCl rate during ramp treatments. R_{Th} is indicated. (*E*) Signaling response to ramp treatments plotted as a function of time. (*F*) AND logic model indicating the order of condition completion for the ramps exceeding R_{Th}. (*G*) Quadratic NaCl concentration change indicating the time that the concentration term (t_C) is satisfied. (*H*) NaCl rate change indicating the time the treatment reaches the rate threshold (t_{RTh}). (*I*) Signaling response to the quadratic treatment depicted in *A* and *B* indicating t_C and t_{RTh}. (*J*) AND logic model for quadratic stimulation.

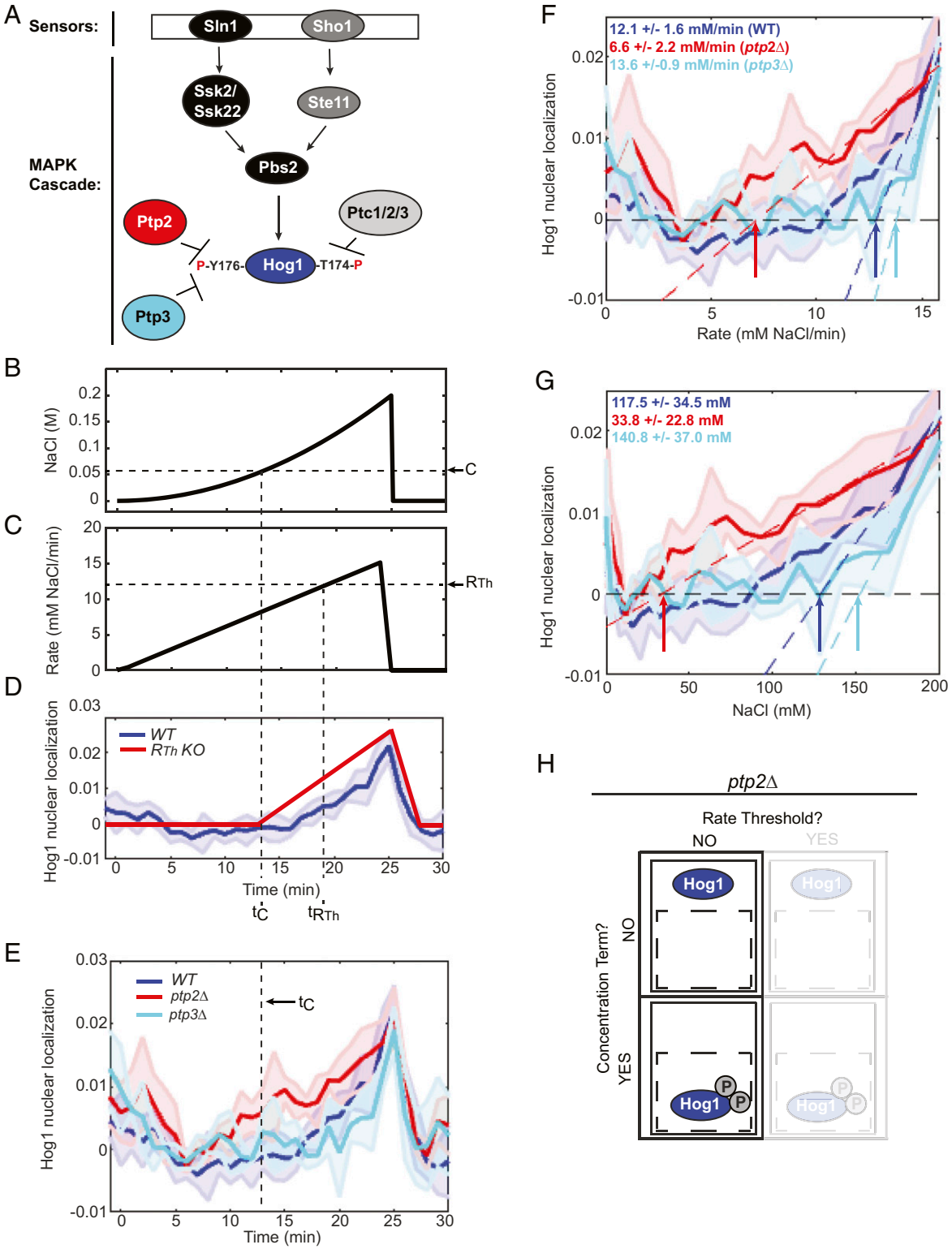

Fig. 3. The rate threshold for Hog1 nuclear localization is specifically dependent on the Ptp2 phosphatase. (*A*) Simplified model of the HOG pathway. Hypothesized regulators of the rate threshold are indicated in red and cyan. (*B*) Quadratic NaCl concentration treatment indicating C and t_C. (*C*) NaCl rate during quadratic treatment with R_{Th} and t_{RTh} marked. The treatment rate at the time C is satisfied can be found at the intersection of the solid black line and the dotted line representing t_C. (*D*) Signaling response to quadratic stimulation in WT (measured, blue) and rate threshold knock out (R_{Th} KO) mutant (predicted, red). t_C and t_{RTh} are marked. (*E*) Signaling response to quadratic treatment in *WT*, *ptp2*Δ, and *ptp3*Δ cells. (*F*) Signaling response in the *WT*, *ptp2*Δ, and *ptp3*Δ strains plotted as a function of NaCl treatment rate. The fitted R_{Th} in each strain is listed in bold type. (*G*) Response in each strain plotted as a function of NaCl concentration. The apparent C in each strain is listed. (*H*) Model of Hog1 activation in the *ptp2*Δ strain indicating the apparent loss of regulation via the rate threshold.

quadratic stimulation, accumulation in *ptp2Δ* cells occurred much earlier (Fig. 3*E*).

Reanalyzing accumulation as a function of rate revealed that accumulation in *ptp2Δ* corresponds with a substantially reduced rate threshold (Fig. 3*F*) compared to *WT*. Further, reanalyzing accumulation as a function of concentration revealed that the timing of nuclear enrichment in *ptp2Δ* corresponds with a concentration that is within error of our measured concentration

A

PTP2 Expression Plasmid	Ptp2 Expression Level	Predicted Rate Threshold	Prediction met? (0.2 M Quadratic)	Prediction met? (0.4 M Quadratic)
empty	none	none	yes	yes
PTP2	normal	normal	yes	yes
ADH1	high	intermediate	?	yes
TEF1	very high	high	?	yes

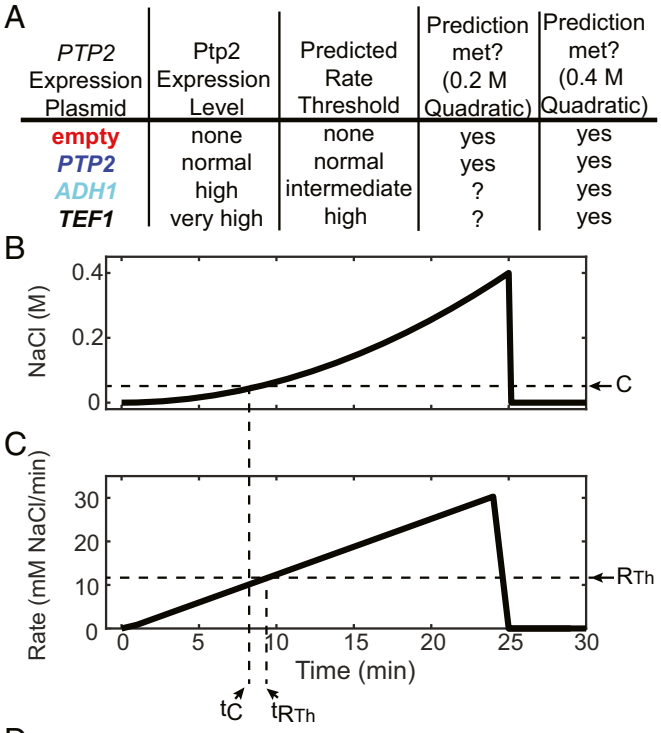

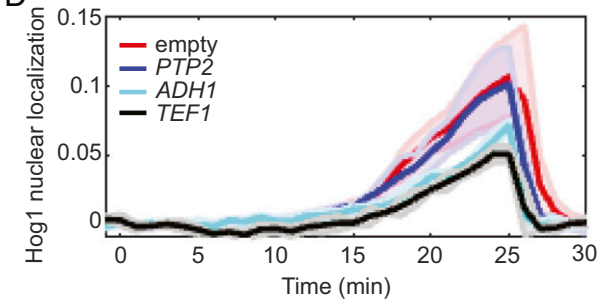

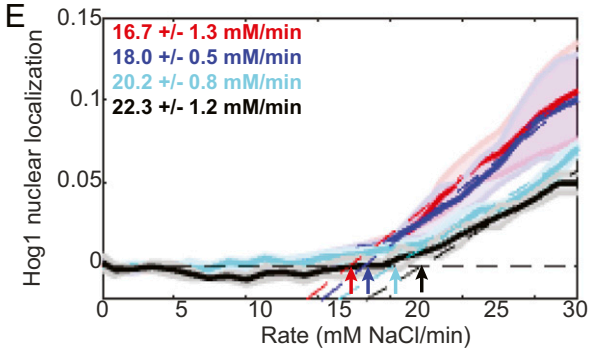

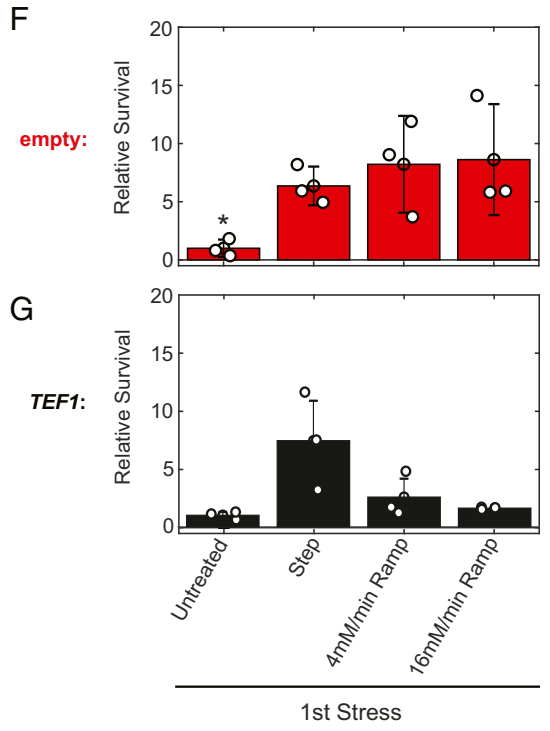

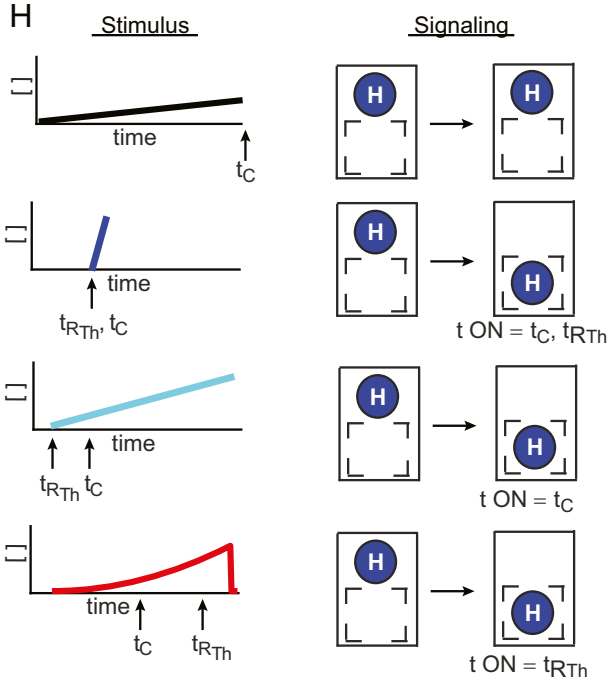

Fig. 4. Ptp2 expression levels fine-tune the stimulation rate required to activate Hog1 signaling. (*A*) Table of predicted rate thresholds as a function of Ptp2 expression level indicating how the quadratic treatment to 0.4 M correspond with the predictions. (*B*) NaCl concentration during a 0.4 M NaCl quadratic stimulation indicating the C and t_C. (*C*) NaCl rate during these stimulations indicating R_{Th} and t_{RTh}. (*D*) Hog1 nuclear localization response to the quadratic stimulation in *A* and *B* depicted as a function of time in each *PTP2* expression strain. (*E*) Signaling response plotted as a function of NaCl treatment rate. The R_{Th} in each strain are indicated in bold. (*F*) High stress survival in the *ptp2Δ* strain containing an empty plasmid. (*G*) High-stress survival in the *ptp2Δ* strain where *PTP2* is expressed using the *TEF1* upstream regulatory DNA. In both *F* and *G*, cells were treated as in Fig. 1*B* and the data are plotted as in Fig. 1*C*. Bars and errors are means and SD from three biological replicates. (*H*) Model showing signaling correspondence with C, R_{Th}, both, or neither depending on stimulation type.

term (57 ± 14.5 mM NaCl) (Fig. 3*G*). These effects are invisible in the Hog1 translocation responses during pulse treatment, which are very similar in *WT*, *ptp2Δ*, and *ptp3Δ* strains (*SI Appendix*, Fig. S9). Thus, finding that nuclear accumulation in *ptp2Δ* cells apparently depends only on the concentration term condition (Fig. 3*H*) required the use of a rate-varying stimulus treatment.

Tuning the Rate Threshold. If Ptp2 indeed serves as a major rate threshold regulator, its overexpression should increase the stimulation rate required for Hog1 nuclear enrichment. Testing this hypothesis requires a series of *PTP2* expression strains. To generate such strains, we constitutively expressed *PTP2* in the *ptp2Δ* strain under the control of the upstream regulatory DNA sequences for other genes (*ADH1* and *TEF1*). This effort resulted in strains with highly increased Ptp2 expression levels (*SI Appendix*, Fig. S10). We anticipated that the empty vector in the *ptp2Δ* strain and the *PTP2* plasmid strain in the *ptp2Δ* strain, which expresses *PTP2* from its native promoter, would phenocopy the *ptp2*Δ and *WT* strains, respectively. We also hypothesized that the induction of Hog1 translocation in *ptp2Δ* strains overexpressing *PTP2* would require a higher rate of stimulus addition than that observed in the *PTP2* plasmid expressing strain in the *ptp2Δ* background. To test these hypotheses, we studied the Hog1 translocation patterns in these strains during quadratic stimulations.

A quadratic treatment delivering rates up to 16 mM/min (*SI Appendix*, Fig. S10 *B* and *C*) induced Hog1 nuclear translocation in the empty vector and *PTP2* plasmid strains in the *ptp2Δ* background, but not in either of the overexpression strains (*SI Appendix*, Fig. S10*D*). Hog1 translocation in the empty vector strain corresponded with a lower rate than the *PTP2* plasmid strain under this stimulation (*SI Appendix*, Fig. S10*E*). These findings agree with our predictions for empty vector and *PTP2* plasmid in the *ptp2Δ* background strains.

Meanwhile, the lack of nuclear accumulation in the overexpression strains could be attributed to either complete suppression of signaling of these strains or the requirement for a stimulation rate greater than those included in the quadratic stimulation tested (Fig. 4*A*). To determine if higher stimulation rates could induce Hog1 translocation in the overexpression strains, we treated our *PTP2* expression strains in the *ptp2Δ* background with a second quadratic gradient that included rates up to 30 mM/min (Fig. 4 *B* and *C*). Because the time between both required thresholds is minimal in this quadratic (Fig. 4 *B* and *C*), we anticipated that unless Ptp2 knockout decreases the concentration term as well as the rate threshold the difference in Hog1 translocation pattern during this treatment between the empty vector and *PTP2* plasmid in the *ptp2Δ* background strains would be minimal. However, the increased rates of addition included in this quadratic could enable Hog1 translocation in the *PTP2* overexpression strains in the *ptp2Δ* background.

Hog1 translocation was observed in all strains under this stimulation pattern (Fig. 4*D*). The pattern of nuclear accumulation in the empty vector and *PTP2* plasmid strains in the *ptp2Δ* background was comparable in this stimulus treatment, as expected based on our AND logic mode (Fig. 4*E*). This result is also consistent with the conservation of the concentration term in the empty vector in the *ptp2Δ* background strain resulting in minimal differences in the observed time of Hog1 activation and minimal difference in the rate thresholds. In addition, these results support our hypothesis that the *PTP2* plasmid strain in the *ptp2Δ* background would phenocopy *WT* yeast (*SI Appendix*, Figs. S7 *C* and *D* and S11). Meanwhile, translocation in the overexpression strains corresponded with higher stimulation rates (Fig. 4*E*). Taken together, the results of our two quadratic stimulations agree with our predictions of *PTP2* expression variant high-stress survival strain behavior (Fig. 4 *F* and *G*).

Finally, we hypothesized that the changes in the stimulus addition rate required to induce Hog1 translocation in our *PTP2* expression strains would alter their survival pattern in our preconditioning protection assay. Specifically, both ramp treatments should promote second high-stress survival in the empty vector strain. Meanwhile, neither ramp should induce high-stress survival in a *PTP2* overexpression strain in the *ptp2Δ* background. As predicted, empty vector strain cell high-stress survival was similar among the pulse and two ramp treatments (Fig. 4*F*), whereas *PTP2* overexpression (*TEF*) cells treated with the two ramps were more sensitive to high-stress than the same cells preconditioned with a pulse (Fig. 4*G*). These results demonstrate that Ptp2 expression levels can affect preconditioning protection as well as fine-tune the rate required to activate signaling and cell survival (Fig. 4*A*).

In summary, the experiments we have presented directly describe regulation of the HOG pathway by a rate threshold whose set point can be modulated by Ptp2 expression levels. Our rate threshold discoveries represent a paradigm shift in the logic of signaling regulation, and in the next section we discuss their implications.

Discussion

Because stimulation patterns vary in terms of both stimulus concentration and rate of addition in vivo (1–7), it is important to thoroughly understand how the rate of stimulation affects signal transduction and resulting cell behavior. Here, we have investigated how stimulation rate impacts the budding yeast Hog1 model MAPK pathway. We find that shallow rates of stimulation that fall below a rate threshold underprepare cells for future high-stress survival, corresponding with a failure to induce signaling. We also find that this rate threshold collaborates with a concentration term in that both conditions must be met in a finite-rate stimulation gradient for signaling to occur.

These findings demonstrate that the timing of activation depends as much upon stimulation rate as it does upon stimulus concentration change. Thus, stimulation profile matters at least as much as stimulus identity in determining whether, when, and to what extent signaling and associated cellular activity occur. Using our innovative application of rate-varying stimulus treatments, we find that signal transduction can correspond with neither, both, or either variable depending on the specific type of stimulus profile applied (Fig. 4*H*). This correspondence pattern appears to exist regardless of the absolute salt concentration baseline (*SI Appendix*, Fig. S4). Meanwhile, signaling pathway mutations, such as the *PTP2* deletion and expression-level variants, may eliminate or alter the rate threshold requirement and preconditioning protection phenotype (Figs. 3 and 4). However, such alterations are invisible under widely utilized switch-like treatments (*SI Appendix*, Fig. S12).

These findings are important because the signaling logic paradigm that controls the yeast osmostress pathway likely also governs other pathways. Given the failure of shallow stimulus gradients to trigger *B. subtilus* general stress and mouse myoblast morphogen signaling even when concentrations are sufficient for activation during pulsed treatment (10, 12), it seems likely that at the minimum these two pathways also operate using an AND logic mechanism. Adapting pathways, which by definition must be sensitive to the changes in stimulus concentration over time (e.g., the rate), should also follow AND logic (1, 2, 40, 47, 3–6, 11–13, 16). Furthermore, any pathway that displays sensitivity to stimulation rate due to its particular activation and deactivation dynamics may be subject to AND regulation (7, 10, 14, 48). We therefore speculate that rate thresholds are a general operating principle of signaling systems, particularly those where known physiological variation in stimulation rate exists (1–7). A general rate threshold logic mechanism carries with it implications for 1) how cells make signaling decisions, 2) experimental design, and 3) apparent redundancy in signaling networks.

Rate threshold logic mechanisms likely set important limits on pathway sensitivity to extracellular stimulation. In the case of the HOG pathway studied here, these limits likely serve the same purpose as the sensitivity limits set by concentration thresholds in many systems (8, 9): conserve cellular resources specifically for significant stressors/stimulations. Slow increases in osmostress may not immediately threaten cell fitness. Consistent with this idea, we do not observe any substantial growth difference between yeast treated with single ramp stimulations above and below the rate threshold (*SI Appendix*, Fig. S1). Rate threshold regulation of osmostress signaling thus appears to ensure an advantageous level of cell sensitivity to stimulation rate. In other pathways, rate threshold mechanisms would provide a helpful way to differentiate signal from noise. The likely rate threshold in the *B. subtilis* general stress pathway (10) probably also helps conserve resources by activating only when the type of stress the cells experience is unclear. Meanwhile, having cells effectively ignore very shallow morphogen gradients, as appears to be the case in the mouse myoblast morphogen signaling pathway, likely helps direct cells into separate fates during development (11, 12).

Because both rate and concentration thresholds set the limits of cellular sensitivity to extracellular stimuli, measuring these conditions in other signaling pathways serves as an essential goal in signaling biology. Having these measurements in hand would enable better understanding and prediction of how cells will respond to a given dynamic stimulation profile. Further, defining the limits of cellular sensitivity would enable the detection of changes in these limits caused by signaling pathway mutations such as those common in cancer and developmental disorders (49). Identifying these aberrant sensitivities would improve our understanding of disease etiology and aid in the design of better treatments. Importantly, the signaling logic paradigm uncovered by our study provides the necessary guide for designing dynamic stimulation profiles that rapidly detect and measure threshold conditions. These profiles are easy to implement and can be readily applied to make threshold condition measurements in any signaling pathway and/or cell type (4, 14, 50).

The existence of any detected threshold condition begs the question of what regulates the condition. We found that in the yeast HOG pathway the protein tyrosine phosphatase Ptp2 serves as one major regulator of our newly discovered rate threshold condition. Excitingly, this function provides Ptp2, which is otherwise partially redundant with Ptp3 (23, 33, 35), with an apparently unique role. Additionally, it expands the list of possible roles for phosphatases, which remain generally much less understood than kinases despite the fact that both types of factors contribute to balancing cellular phosphorylation levels (51). While phosphatases have been thought of as pathway on/off switches, our findings and those of another pioneering study performed using bacterial two-component systems (52) show that these important signaling factors can regulate cellular sensitivity to extracellular stimulation. Further investigations using dynamic stimulation profiles are needed to determine whether phosphatases in other signaling systems regulate cellular sensitivity to stimulus concentration and rate of addition. Such studies may also enable the identification of unique functions for specific phosphatases as well as other factors that appear redundant or partially redundant during switch-like changes in stimulus concentration, thereby facilitating the disentanglement of complex signaling networks.

In conclusion, we have demonstrated a rate threshold mechanism in the HOG pathway along with a highly generalizable strategy for investigating threshold conditions and the signaling pathway components that regulate them. Given the complexity in the signaling pattern seen in the Hog1 pathway, we expect that concentration and rate thresholds are only some of the mechanisms that contribute to signaling dynamics in the Hog1 pathway. Therefore, it is likely that other signaling mechanisms will be discovered in the future through specific combinations of different dynamic stimulation profiles. We strongly anticipate that the application of this strategy to other systems will transform our understanding of the logic underlying the complex signaling networks present in higher eukaryotes and possibly even enable improved disease diagnosis and treatment.

Materials and Methods

Yeast Constructs and Strains. All plasmids used in this study (*SI Appendix*, Table S1) were constructed via standard restriction enzyme cloning. Appropriate restriction sites were either included in custom synthesized oligonucleotides (IDT) or introduced by PCR with Q5 High-Fidelity Polymerase (NEB) according to the manufacturer's instructions. All constructs were sequence-verified.

The yeast strains used in this study (*SI Appendix*, Table S2) were derived from the haploid *S. cerevisiae* BY4741 strain (53). All yeast genomic deletions and integrations were confirmed via PCR. The *PTP2* and *PTP3* genes have been replaced with the kanamycin resistance cassette (*KANMX4*) in the *ptp2*Δ and *ptp3*Δ strains (54). Strains used to track Hog1-YFP nuclear localization were obtained from a previous study (40) or generated by C-terminally tagging the endogenous *HOG1* with sequences encoding YFP (33) through homologous DNA recombination. Ptp2 expression and empty vector control plasmids were introduced into yeast via high-efficiency yeast transformation (55).

Yeast Growth. Three days before an experiment, yeast cells from a glycerol stock stored at −80 °C were streaked out on Complete Synthetic Media (CSM) (Formedium) or CSM lacking uracil (CSM-Ura) (Formedium) for selection as needed. The day before the experiment, a single colony from the plate was inoculated in liquid media (preculture). After 2 to 6 h, the optical density at 600 nm (OD_{600}) of the preculture was measured and diluted into fresh liquid culture to reach an OD_{600} of 0.3 to 0.5 (depending on the experimental application) the next morning. These OD_{600} values represent 1.5 to 2.5 × 10^6 cells per mL.

Pump Profile Generation. Pump profiles designed to deliver varying rate salt treatments were generated using an in-house-developed MATLAB script that accounts for stock NaCl concentration, pump withdraw rate, volume in the container in which the profile is generated, and culture volume change (14). Profiles were loaded onto programmable syringe pumps (New Era Pump Systems) prior to treatment.

High-Stress Preconditioning Assay. High-stress preconditioning assays were designed based on previous work (43, 44). Initial stress treatments began when cells in culture grown overnight reached an OD_{600} of 0.3. The untreated and 1-h 0.4 M NaCl pulse first stress treatments were chosen as negative and positive controls. Ramp treatments were delivered directly to cells in culture via tubing connecting culture flasks to stock CSM NaCl solution placed in programmable syringe pumps (New Era Pump Systems). These treatments were designed in order to deliver salt at a rate of either 4 mM NaCl/min or 16 mM NaCl/min to a final concentration of 0.4 M NaCl. The time each ramp treatment was held at 0.4 M NaCl was determined such that all first stress treatments that included NaCl received the same cumulative salt exposure (see calculations below). Because treatment duration varied, first stress treatment start times were adjusted such that all treatments ended at the same time. Upon completion of the first treatment, culture OD_{600} was measured and 14 mL of each culture was transferred to 15-mL conical tubes, and cells were harvested by centrifugation for 5 min at 3,000 × *g*. The supernatant was removed, and cells were resuspended in 1 mL sterile H_2O, transferred to 1.5-mL microcentrifuge tubes (Eppendorf), and pelleted by centrifugation for 5 min at 21,300 × *g*. Supernatant was removed and pellets were resuspended in 100 μL sterile H_2O. Five microliters of each resuspended culture was transferred to 145 μL of either CSM (0 M NaCl second stress) or 2 M NaCl CSM (high second stress) in the first well of each row of a 96-well plate. Once all cultures were transferred, each was diluted 1:2 across the wells of each plate column containing 100 μL of each second stress treatment. Ninety-six-well plates were incubated at 30 °C with shaking at 250 rpm for 2.5 h. After this time, 150 μL CSM was added to each well. Culture in the wells was spotted using a replica plater (Sigma R2508) onto a 15-cm 2% agar CSM plate to enable the determination of relative high-stress survival. To quantitate differences in high second stress survival, culture from the first well of each row (containing the highest concentration of cells from each sample) was diluted 1:2,000, and 600 μL of each treatment was spread onto a 15-cm 2% agar CSM plate.

Plates were incubated for 2 to 3 d at 30 °C and imaged using a ChemiDoc MP (Bio-Rad). Individual colonies from the plates generated to enable high second stress survival quantitation were counted using in-house-developed MATLAB scripts. In brief, after the user is prompted to define the plate diameter by clicking, the scripts process the plate images to generate a uniform background. The image is converted to binary with the background and colonies converted into opposite values and the number of centroids within a user-defined size range in the binary colony value are recorded.

For each first stress treatment, survival was calculated manually by dividing the number of colonies formed from culture exposed to the 2 M NaCl second stress by the number formed from exposure to 0 M NaCl second stress. Relative survival mean and SD were calculated by normalizing the survival resulting from each first stress to mean survival in the untreated first stress culture for three independent biological replicates. Statistical significance was calculated using the Kolmogorov–Smirnov test.

Example cumulative salt exposure calculation:

$$Cumulative\ exposure = NaCl_{max}\left[\int_{t=0}^{t=t_{max}} f(t)dt + (t_{end} - t_{max})\right],$$

where $f(t)$ = profile function, $NaCl_{max}$ = maximum NaCl concentration, t_{max} = time to reach maximum NaCl exposure, and t_{end} = end of the treatment.

Example: linear gradient to 0.4 M in 100 min; $f(t) = t$; t_{max} =100 min; $NaCl_{max}$ = 0.4 M, and t_{end} = 110 min:

$$Cumulative\ exposure = 0.4\ \text{M}\left[\int_{t=0}^{t=100} t * dt + (110\ \text{min} - 100\ \text{min})\right]$$
$$= 0.4\ \text{M} * \left(\frac{100\ \text{min}}{2}\right) + 0.4\ \text{M} * 10\ \text{min} = 24\ \text{M} * \text{min}$$

Time-Lapse Microscopy.

Treatments. Three milliliters of yeast cells expressing *HOG1-YFP* from the chromosome grown to an OD_{600} of 0.45 to 0.55 (2.25 to 2.75 × 10^6 cells per mL) were pelleted by centrifugation at 500 × *g* for 6 min. Cell pellets were resuspended in 50 μL CSM and loaded into a flow chamber as previously described (18). Three types of perturbations were used in time-lapse microscopy treatments: pulse, linear ramp, and quadratic gradients. To deliver the pulse treatments, flow chambers containing cells were connected via tubing to a conical tube containing the CSM NaCl treatment to be delivered on one end and a programmable syringe pump (New Era Pump Systems) set to withdraw media on the other. Ramp and quadratic perturbations were set up as described previously (14). In brief, these perturbations were generated in a beaker containing CSM subjected to constant mixing on a stir plate by delivering CSM NaCl stock solution in preprogrammed steps via syringe pump (New Era Pump Systems). Media was drawn from this beaker to the flow chamber over the time course of treatment profile generation using a syringe pump programmed to withdraw media at a rate of 0.1 mL/min. At the completion of all NaCl treatments, cells were returned to CSM by switching the beaker or conical containing CSM NaCl to a conical containing CSM only. For the precondition experiments cells are grown in 0.2 M NaCl for 24 h prior to time-lapse microscopy. Cells are then loaded into the flow chamber for time-lapse microcopy experiments applying different step, ramp, or quadratic treatments.

Image acquisition. The Micro-Manager program (https://micro-manager.org/) version 1.4 was used to control a Nikon Ti Eclipse epifluorescent microscope equipped with perfect focus (Nikon), a 100× VC DIC lens (Nikon), a fluorescent filter for YFP (Semrock), an X-cite fluorescent light source (Excelitas), and an Orca Flash 4v2 CMOS camera (Hamamatsu). YFP images were collected every 1 min with an exposure of 20 ms. Bright-field (TRANS) images with an exposure of 10 ms were collected every 10 s during each time-lapse experiment. Three or four YFP images of cells loaded on the flow chamber were taken prior to the start of each treatment to enable Hog1 nuclear localization baseline level determination.

Image analysis. Image segmentation was performed in two steps. First, YFP images (detecting Hog1-YFP) were smoothed and background-corrected. A threshold was set to identify the brightest pixels for each cell. The region containing the 100 brightest pixels in each cell was then used as an intracellular marker. Second, TRANS images were smoothed, background-corrected, and overlain with the corresponding YFP image (or the YFP image from the previous time point in the case were no YFP image was taken). A watershed algorithm was applied to these overlain images to segment and label the objects (cells). After segmentation, objects that deviate significantly in size from the average cell or on the border of the image are removed, resulting in an image with segmented cells. This process was repeated for each image. After segmentation, the centroid of each cell was computed and stored. The distances between the centroids of each cell in consecutive images were compared. The centroids that show the smallest distance difference between two consecutive images are considered the same cell at two different time points. This whole procedure is repeated for each image, resulting in single-cell trajectories. Each single-cell trace was visually inspected, and cells exhibiting large fluctuations in YFP or TRANS signal over the time course were removed. In a typical experiment, 20 to 30% of a starting population of 200 to 450 single cells remained after this filtering step for further processing.

To determine Hog1 nuclear localization in each cell, the average per-pixel fluorescent intensity of the whole cell (I_w) and of the top 100 brightest fluorescent pixels (I_t) was calculated. In addition, fluorescent signal per pixel of the camera background (I_b) was recorded. Hog1 nuclear localization was calculated as $\text{Hog1}(t) = [(I_t(t) - I_b)/(I_w(t) - I_b)]$. The value for $\text{Hog1}(t = 0)$ defines Hog1 nuclear localization baseline level. Single-cell traces were smoothed and nuclear localization over the time course was determined by subtracting $\text{Hog1}(t = 0)$ from $\text{Hog1}(t)$. For cell volume measurements, volume change relative to the volume at the beginning of the experiment was calculated. For both the single-cell volume and Hog1(t) fluorescent traces, the median and the average median distance (the equivalent of the SD if the median is used instead of the mean) were computed to put less weight on sporadic outlier cells due to the image segmentation process.

The in-house-developed codes used for image segmentation (56) and time-lapse image analysis (14, 41, 57) have been previously described.

Determination of concentration and rate thresholds. The rate and concentration thresholds were determined by plotting the median Hog1 nuclear localization in each biological replicate as a function of treatment concentration or rate, respectively. Two points were manually selected from each of these plots demarcating the beginning and end point of robust Hog1 nuclear enrichment. The data between these points was automatically fit to the linear function (y = mx + b). The "x" value (concentration or rate) at the intersection point of a horizontal line at Hog1 = 0 (baseline) and the line fitting Hog1 nuclear enrichment pattern (activation) was determined. The average and SD of the "x" values from the replicates for each treatment profile represent the concentration and rate thresholds corresponding with Hog1 nuclear localization in those treatment profiles. The average slope ("m") and y-intercept ("b") from the linear function fit to the Hog1 activation data for each biological replicate obtained from a particular treatment profile were used to generate the dotted lines overlaying Hog1 nuclear enrichment in the threshold determination figures.

Immunoblotting. Mild alkali treatment and heating in standard electrophoresis buffer (58) were used to extract total protein from yeast cell pellets containing 1 OD_{600} unit (5 × 10^6 cells). Proteins were fractionated on a NuPAGE 4 to 12% Bis-Tris denaturing polyacrylamide gel (Thermo Fisher Scientific). Gels were equilibrated in transfer buffer (30 mM bicine, 25 mM Bis-Tris, 1 mM EDTA, and 60 μM chlorobutanol) and electrotransferred to Polyvinylidene difluoride (PVDF) membranes preequilibrated in transfer buffer (Immobilon-P. 0.45 μM; GE); 5% wt/vol nonfat milk in 1× Tris-buffered saline (TBS) (100 mM Tris·Cl, pH 7.5, and 150 mM NaCl) was used for blocking. HAx3-Ptp2 was detected using an anti-hemagglutinin (HA) horseradish peroxidase (HRP) conjugate 3F10 (Roche) at a 1:5,000 dilution. Endogenous actin (used as a loading control) was detected using a 1:5,000 dilution of anti–β-actin antibody (ab8224; Abcam) followed by incubation with a 1:2,500 dilution of HRP-conjugated horse anti-mouse immunoglobulin G (IgG) antibody (7076S; Cell Signaling). All antibody incubations were performed in 1% wt/vol nonfat milk blocking in 1× TBS. Antibody signals were visualized using. Enhanced chemiluminescence (ECL) reagent (GE) was used to detect antibody signals. Signals were visualized using a ChemiDoc MP Imaging System (Bio-Rad).

Data and Code Availability. The datasets generated during the current study are included for each figure and have been deposited as Dataset S1 at http://dx.doi.org/10.17632/ms9y3wdjjc.1. Cell segmentation codes have been previously described (56) and are available in the public OSF repository: https://osf.io/kwbe6/. Image processing codes have also been previously described (14, 41, 57). All codes used for image processing and analysis in this study are available at https://osf.io/kwbe6/.

ACKNOWLEDGMENTS. We thank Mr. Cleland, Mr. Hughes, Mr. Venkat, and Drs. Weil, Tansey, Wadzinski, Carrasco, and Colbran for feedback on the study and manuscript. We would also like to thank the Vanderbilt Molecular Biology core facility for providing access to and technical assistance with instrumentation necessary to complete this work. This work was supported

by the NIH Director's New Innovator Award (1DP2GM114849), the National Institute of General Medical Sciences (5R01GM115892), the Advanced Computing Center for Research and Education (1S10OD023680-01), and Vanderbilt University Startup Funds. A.N.J. was supported by the Ion Channels and Transporters Training Grant (T32NS007491), B.K.K. was supported by the Molecular Biophysics Training Grant (5T32GM008320) and A.T. was supported by an American Heart Association predoctoral fellowship (18PRE34050016). The content of this publication is solely the responsibility of the authors and does not necessarily represent the official views of the NIH.

1. K. S. Polonsky, B. D. Given, E. Van Cauter, Twenty-four-hour profiles and pulsatile patterns of insulin secretion in normal and obese subjects. *J. Clin. Invest.* **81**, 442–448 (1988).
2. E. K. Hoffmann, I. H. Lambert, S. F. Pedersen, Physiology of cell volume regulation in vertebrates. *Physiol. Rev.* **89**, 193–277 (2009).
3. R. Chovatiya, R. Medzhitov, Stress, inflammation, and defense of homeostasis. *Mol. Cell* **54**, 281–288 (2014).
4. T. S. Shimizu, Y. Tu, H. C. Berg, A modular gradient-sensing network for chemotaxis in Escherichia coli revealed by responses to time-varying stimuli. *Mol. Syst. Biol.* **6**, 382 (2010).
5. C. J. Wang, A. Bergmann, B. Lin, K. Kim, A. Levchenko, Diverse sensitivity thresholds in dynamic signaling responses by social amoebae. *Sci. Signal.* **5**, ra17 (2012).
6. G. Brabant, K. Prank, C. Schofl, Pulsatile patterns in hormone secretion. *Trends Endocrinol. Metab.* **3**, 183–190 (1992).
7. A. Sagner, J. Briscoe, Morphogen interpretation: Concentration, time, competence, and signaling dynamics. *Wiley Interdiscip. Rev. Dev. Biol.* **6**, e271 (2017).
8. K. E. Forsten, D. A. Lauffenburger, Autocrine ligand binding to cell receptors. Mathematical analysis of competition by solution "decoys". *Biophys. J.* **61**, 518–529 (1992).
9. J. Ang, E. Harris, B. J. Hussey, R. Kil, D. R. McMillen, Tuning response curves for synthetic biology. *ACS Synth. Biol.* **2**, 547–567 (2013).
10. J. W. Young, J. C. W. Locke, M. B. Elowitz, Rate of environmental change determines stress response specificity. *Proc. Natl. Acad. Sci. U.S.A.* **110**, 4140–4145 (2013).
11. I. Heemskerk *et al.*, Rapid changes in morphogen concentration control self-organized patterning in human embryonic stem cells. *eLife* **8**, e40526 (2019).
12. B. Sorre, A. Warmflash, A. H. H. Brivanlou, E. D. Siggia, Encoding of temporal signals by the TGF-β pathway and implications for embryonic patterning. *Dev. Cell* **30**, 334–342 (2014).
13. H. Kubota *et al.*, Temporal coding of insulin action through multiplexing of the AKT pathway. *Mol. Cell* **46**, 820–832 (2012).
14. A. Thiemicke, H. Jashnsaz, G. Li, G. Neuert, Generating kinetic environments to study dynamic cellular processes in single cells. *Sci. Rep.* **9**, 10129 (2019).
15. K. A. Fujita *et al.*, Decoupling of receptor and downstream signals in the Akt pathway by its low-pass filter characteristics. *Sci. Signal.* **3**, ra56 (2010).
16. S. Sasagawa, Y. Ozaki, K. Fujita, S. Kuroda, Prediction and validation of the distinct dynamics of transient and sustained ERK activation. *Nat. Cell Biol.* **7**, 365–373 (2005).
17. Y. Goulev *et al.*, Nonlinear feedback drives homeostatic plasticity in H_2O_2 stress response. *eLife* **6**, e23971 (2017).
18. D. Muzzey, C. A. Gómez-Uribe, J. T. Mettetal, A. van Oudenaarden, A systems-level analysis of perfect adaptation in yeast osmoregulation. *Cell* **138**, 160–171 (2009).
19. Y. Tu, T. S. Shimizu, H. C. Berg, Modeling the chemotactic response of Escherichia coli to time-varying stimuli. *Proc. Natl. Acad. Sci. U.S.A.* **105**, 14855–14860 (2008).
20. J. L. Brewster, M. C. Gustin, Hog1: 20 years of discovery and impact. *Sci. Signal.* **7**, re7 (2014).
21. J. L. Brewster, T. de Valoir, N. D. Dwyer, E. Winter, M. C. Gustin, An osmosensing signal transduction pathway in yeast. *Science* **259**, 1760–1763 (1993).
22. P. J. Westfall, D. R. Ballon, J. Thorner, When the stress of your environment makes you go HOG wild. *Science* **306**, 1511–1512 (2004).
23. H. Saito, F. Posas, Response to hyperosmotic stress. *Genetics* **192**, 289–318 (2012).
24. P. Ferrigno, F. Posas, D. Koepp, H. Saito, P. A. Silver, Regulated nucleo/cytoplasmic exchange of HOG1 MAPK requires the importin beta homologs NMD5 and XPO1. *EMBO J.* **17**, 5606–5614 (1998).
25. J. G. English *et al.*, MAPK feedback encodes a switch and timer for tunable stress adaptation in yeast. *Sci. Signal.* **8**, ra5 (2015).
26. V. Reiser, H. Ruis, G. Ammerer, Kinase activity-dependent nuclear export opposes stress-induced nuclear accumulation and retention of Hog1 mitogen-activated protein kinase in the budding yeast Saccharomyces cerevisiae. *Mol. Biol. Cell* **10**, 1147–1161 (1999).
27. J. Macia *et al.*, Dynamic signaling in the Hog1 MAPK pathway relies on high basal signal transduction. *Sci. Signal.* **2**, ra13 (2009).
28. A. A. Granados *et al.*, Distributing tasks via multiple input pathways increases cellular survival in stress. *eLife* **6**, e21415 (2017).
29. A. Mitchell, P. Wei, W. A. Lim, Oscillatory stress stimulation uncovers an Achilles' heel of the yeast MAPK signaling network. *Science* **350**, 1379–1383 (2015).
30. P. Hersen, M. N. McClean, L. Mahadevan, S. Ramanathan, Signal processing by the HOG MAP kinase pathway. *Proc. Natl. Acad. Sci. U.S.A.* **105**, 7165–7170 (2008).
31. P. J. Westfall, J. C. Patterson, R. E. Chen, J. Thorner, Stress resistance and signal fidelity independent of nuclear MAPK function. *Proc. Natl. Acad. Sci. U.S.A.* **105**, 12212–12217 (2008).
32. P. J. Westfall, J. Thorner, Analysis of mitogen-activated protein kinase signaling specificity in response to hyperosmotic stress: use of an analog-sensitive HOG1 allele. *Eukaryot. Cell* **5**, 1215–1228 (2006).
33. S. M. Wurgler-Murphy, T. Maeda, E. A. Witten, H. Saito, Regulation of the Saccharomyces cerevisiae HOG1 mitogen-activated protein kinase by the PTP2 and PTP3 protein tyrosine phosphatases. *Mol. Cell. Biol.* **17**, 1289–1297 (1997).
34. J. Warmka, J. Hanneman, J. Lee, D. Amin, I. Ota, Ptc1, a type 2C Ser/Thr phosphatase, inactivates the HOG pathway by dephosphorylating the mitogen-activated protein kinase Hog1. *Mol. Cell. Biol.* **21**, 51–60 (2001).
35. C. P. Mattison, I. M. Ota, Two protein tyrosine phosphatases, Ptp2 and Ptp3, modulate the subcellular localization of the Hog1 MAP kinase in yeast. *Genes Dev.* **14**, 1229–1235 (2000).
36. T. Maeda, S. M. Wurgler-Murphy, H. Saito, A two-component system that regulates an osmosensing MAP kinase cascade in yeast. *Nature* **369**, 242–245 (1994).
37. C. Young, J. Mapes, J. Hanneman, S. Al-Zarban, I. Ota, Role of Ptc2 type 2C Ser/Thr phosphatase in yeast high-osmolarity glycerol pathway inactivation. *Eukaryot. Cell* **1**, 1032–1040 (2002).
38. T. Jacoby *et al.*, Two protein-tyrosine phosphatases inactivate the osmotic stress response pathway in yeast by targeting the mitogen-activated protein kinase, Hog1. *J. Biol. Chem.* **272**, 17749–17755 (1997).
39. H. Martín, M. Flández, C. Nombela, M. Molina, Protein phosphatases in MAPK signalling: We keep learning from yeast. *Mol. Microbiol.* **58**, 6–16 (2005).
40. J. T. Mettetal, D. Muzzey, C. Gómez-Uribe, A. van Oudenaarden, The frequency dependence of osmo-adaptation in Saccharomyces cerevisiae. *Science* **319**, 482–484 (2008).
41. G. Neuert *et al.*, Systematic identification of signal-activated stochastic gene regulation. *Science* **339**, 584–587 (2013).
42. J. G. Lewis, R. P. Learmonth, K. Watson, Induction of heat, freezing and salt tolerance by heat and salt shock in Saccharomyces cerevisiae. *Microbiology (Reading)* **141**, 687–694 (1995).
43. D. B. Berry, A. P. Gasch, Stress-activated genomic expression changes serve a preparative role for impending stress in yeast. *Mol. Biol. Cell* **19**, 4580–4587 (2008).
44. D. B. Berry *et al.*, Multiple means to the same end: The genetic basis of acquired stress resistance in yeast. *PLoS Genet.* **7**, e1002353 (2011).
45. S. Pelet *et al.*, Transient activation of the HOG MAPK pathway regulates bimodal gene expression. *Science* **332**, 732–735 (2011).
46. M. Bell, D. Engelberg, Phosphorylation of Tyr-176 of the yeast MAPK Hog1/p38 is not vital for Hog1 biological activity. *J. Biol. Chem.* **278**, 14603–14606 (2003).
47. H. Chang, A. Levchenko, Adaptive molecular networks controlling chemotactic migration: Dynamic inputs and selection of the network architecture. *Philos. Trans. R. Soc. Lond. B Biol. Sci.* **368**, 20130117 (2013).
48. H. Kubota, S. Uda, F. Matsuzaki, Y. Yamauchi, S. Kuroda, In vivo decoding mechanisms of the temporal patterns of blood insulin by the insulin-AKT pathway in the liver. *Cell Syst.* **7**, 118–128.e3 (2018).
49. W. Lim, B. Mayer, T. Pawson, *Cell Signaling: Principles and Mechanisms* (Garland Science, ed. 1, 2015).
50. C. S. Mokashi, D. L. Schipper, M. A. Qasaimeh, R. E. C. Lee, A system for analog control of cell culture dynamics to reveal capabilities of signaling networks. *iScience* **19**, 586–596 (2019).
51. S. Fahs, P. Lujan, M. Köhn, Approaches to study phosphatases. *ACS Chem. Biol.* **11**, 2944–2961 (2016).
52. B. P. Landry, R. Palanki, N. Dyulgyarov, L. A. Hartsough, J. J. Tabor, Phosphatase activity tunes two-component system sensor detection threshold. *Nat. Commun.* **9**, 1433 (2018).
53. C. B. Brachmann *et al.*, Designer deletion strains derived from Saccharomyces cerevisiae S288C: A useful set of strains and plasmids for PCR-mediated gene disruption and other applications. *Yeast* **14**, 115–132 (1998).
54. E. A. Winzeler *et al.*, Functional characterization of the S. cerevisiae genome by gene deletion and parallel analysis. *Science* **285**, 901–906 (1999).
55. R. D. Gietz, R. A. Woods, Transformation of yeast by lithium acetate/single-stranded carrier DNA/polyethylene glycol method. *Methods Enzymol.* **350**, 87–96 (2002).
56. B. Kesler, G. Li, A. Thiemicke, R. Venkat, G. Neuert, Automated cell boundary and 3D nuclear segmentation of cells in suspension. *Sci. Rep.* **9**, 10237 (2019).
57. B. Munsky, G. Li, Z. R. Fox, D. P. Shepherd, G. Neuert, Distribution shapes govern the discovery of predictive models for gene regulation. *Proc. Natl. Acad. Sci. U.S.A.* **115**, 7533–7538 (2018).
58. V. V. Kushnirov, Rapid and reliable protein extraction from yeast. *Yeast* **16**, 857–860 (2000).